

The Observer as a Local Breakdown of Atemporality: Relational Time and an Informational Arrow from Quantum Clocks

Gabriel Giani Moreno

Revised manuscript — February 2026

Abstract

We present an operational and falsifiable framework in which temporal structure is not fundamental, but emerges from correlations within a globally stationary quantum state. Building on the Page–Wootters (PaW) mechanism, we formalize a minimal set of postulates (P0–P4) that (i) recover effective Schrödinger dynamics for a subsystem conditioned on a physical clock, (ii) quantify clock quality under finite-dimensional and quasi-ideal clocks, and (iii) derive an informational arrow of time as the monotonic (in expectation) growth of an effective entropy for observers with incomplete access to environmental degrees of freedom. A central result is that the three pillars of the problem of time — quantum dynamics, thermodynamic irreversibility, and relativistic frame dependence — arise as three facets of a single conditional operation: projection onto clock states yields dynamics, partial trace over inaccessible degrees of freedom yields the arrow, and the locality of the physical clock yields frame dependence, all from the same timeless global state. The central thesis is that the observer is not a privileged entity in the universe, but a local physical configuration in which global atemporality becomes operationally broken: time and its arrow arise only inside the observer’s coarse-grained description. A minimal demonstrator (clock + qubit + environment) reproduces coherent conditional dynamics in the absence of an environment, and effective decoherence with increasing entropy when inaccessible degrees of freedom are introduced. The robustness of the informational arrow is established through six numerical stress tests — gravitational back-reaction, fuzzy system–environment boundaries, clock uncertainty, Poincaré recurrences, Haar-random initial states, and partition independence — all of which the arrow survives. Finally, both Pillar 1 (pure dynamics) and Pillar 2 (entropy growth) are experimentally validated on IBM Quantum hardware (`ibm_torino`, 133 superconducting qubits): the hardware-measured S_{eff} reaches 0.583 ± 0.005 across three independent runs (102.2% of exact), with device noise fully characterised ($T_1 \approx 148 \mu\text{s}$, two-qubit gate error 0.25%, readout error 4.49%). The framework is positioned within recent advances on temporal quantum reference frames, quasi-ideal clocks, and multi-observer emergent time.

Keywords: relational time; Page–Wootters; quantum clocks; temporal reference frames; decoherence; arrow of time; information; foundations.

Introduction

The “problem of time” appears at the intersection of (i) relativity, where time is observer-dependent and spacetime is dynamical, (ii) quantum theory, where dynamics is typically parameterized by an external time, and (iii) thermodynamics, where an arrow of time emerges despite microscopic reversibility. A standard diagnostic is that these tensions persist not because we lack a better definition of t , but because we frequently treat time as a fundamental background even when our most successful theories already deny a global “now”. In this work, time is not a primitive parameter but an emergent label arising from conditioned descriptions under partial access.

This work takes a deliberately operational stance: a theory of time must specify who can access what information, and under which physical constraints. We argue that once this is made explicit, two statements become natural and testable:

1. **Relational time:** effective evolution arises as a conditional structure within a globally stationary state.
2. **Informational arrow:** irreversibility is not a property of the global state, but of the observer’s restricted description; the arrow emerges from the growth of an effective entropy under partial trace.

A central finding of this work is that these two statements — together with observer-dependent time — are not independent results, but three aspects of a single mathematical operation. The conditional reduced state

$$\rho_S(t) = \frac{\text{Tr}_E[\langle t|_C |\Psi\rangle\langle\Psi| |t\rangle_C]}{p(t)}$$

contains all three: the projection $\langle t|_C$ onto the clock yields dynamics; the partial trace Tr_E yields irreversibility; and the fact that C is a local physical subsystem (not an absolute parameter) yields observer-dependent time. Three pillars, one formula, one timeless global state.

We develop these claims as a compact postulate set (P0–P4), then implement a minimal demonstrator model.

Related Work and Positioning

Our framework is aligned with, and extends, three active research lines:

(i) Temporal quantum reference frames and operational meaning of measurements.

Hausmann et al. compare consistent PaW formulations and clarify the operational meaning of evolution and measurement events relative to temporal quantum reference frames .

(ii) Finite and quasi-ideal clocks, interactions, and effective non-linear dynamics.

Mendes et al. study PaW with gravitational interaction between system and finite-dimensional quasi-ideal clocks, deriving effective Schrödinger-like and non-linear equations with clock-induced decoherence .

(iii) Informational arrows of time in extended PaW models.

Shaari extends a two-qubit PaW setting by introducing auxiliary degrees of freedom to model the observer's incomplete access, leading to growth of an effective entropy and an informational arrow .

We additionally note recent multi-observer emergent-time proposals that unify relativistic and cosmological regimes in a relational framework .

Our contribution is not to re-introduce PaW, quasi-ideal clocks, or informational arrows separately, but to provide an integrated operational pipeline (P0–P4) plus a minimal demonstrator linking: conditional dynamics \leftrightarrow clock quality \leftrightarrow observer-limited access \leftrightarrow informational arrow. We further articulate the ontological reading that the observer corresponds to a local physical regime in which global atemporality becomes operationally broken.

Postulates (P0–P4)

We adopt a minimal postulate set to keep the framework explicit and falsifiable.

P0 — Global Atemporality (Constraint Form)

There exists a global state $|\Psi\rangle$ satisfying a stationarity constraint:

$$\hat{\mathcal{C}} |\Psi\rangle = 0,$$

where $\hat{\mathcal{C}}$ is a global constraint operator (e.g., $\hat{\mathcal{C}} = \hat{H}_C + \hat{H}_S + \hat{H}_E$ up to additive shifts). For finite-dimensional or quasi-ideal clocks, this condition is satisfied

approximately, in the sense that $\|\hat{\mathcal{C}}|\Psi\rangle\|$ is negligible within the operational support of the clock. Exact cancellation is recovered only in the infinite-resolution limit.

P1 — Factorization is a Choice (Operational Partition)

A partition $\mathcal{H} = \mathcal{H}_C \otimes \mathcal{H}_S \otimes \mathcal{H}_E$ is not assumed to be ontologically fundamental, but is an operational choice defining what counts as clock, system, and inaccessible environment for an observer.

P2 — Relational Time via Conditioning (Internal Clock Readout)

Let $|t\rangle_C$ be a clock readout (ideal or approximate). The conditional system state is defined by

$$\rho_S(t) \propto \text{Tr}_{CE}\left[\left(|t\rangle\langle t|_C \otimes \mathbb{I}_{SE}\right)\rho_{CSE}\right],$$

with normalization by the probability $p(t)$. Effective dynamics arises from correlations between C and S inside $|\Psi\rangle$.

P3 — Emergent Schrödinger Dynamics (Good-Clock Regime)

When the clock resolution dt is small compared to the characteristic timescale of \hat{H}_S (i.e., $dt \ll 2\pi/\|\hat{H}_S\|$), and the clock dimension N is sufficiently large to admit a controlled continuum limit $t_k = k dt$, the conditional state approximately satisfies

$$i \frac{\partial}{\partial t} |\psi_S(t)\rangle \approx \hat{H}_S |\psi_S(t)\rangle,$$

or its mixed-state generalization, with deviations controlled by clock imperfection and back-action.

P4 — Informational Arrow from Partial Access

For an observer with incomplete access to E , define an effective entropy

$$S_{\text{eff}}(t) := -\text{Tr}[\rho_S(t) \ln \rho_S(t)].$$

Even when the global evolution is stationary/unitary, $S_{\text{eff}}(t)$ can grow monotonically in expectation for typical coarse-grainings and sufficiently large environments. Residual oscillations and recurrences are expected for finite environments but are suppressed as

the effective environment dimension $d_E = 2^{n_{\text{env}}}$ increases: heuristically, the Poincaré recurrence timescale grows as $\sim d_E$, while the relaxation timescale of S_{eff} scales as $\sim 1/(g^2 d_E)$, so for $n_{\text{env}} \gg 1$ the entropy plateau is reached well before recurrences become significant.

Unified Reading: Three Pillars from a Single Conditional State

The core expression of the framework is the conditional reduced state of the system:

$$\rho_S(t) = \frac{\text{Tr}_E[\langle t|_C |\Psi\rangle \langle\Psi| |t\rangle_C]}{p(t)}, \quad p(t) = \text{Tr}_{SE}[\langle t|_C |\Psi\rangle \langle\Psi| |t\rangle_C].$$

This single operation unifies three traditionally separate pillars of the problem of time:

1. **Quantum dynamics (P3).** The map $t \mapsto \rho_S(t)$, obtained by projecting onto successive clock states $\langle t|_C$, reproduces effective Schrödinger evolution $i \partial_t |\psi_S(t)\rangle \approx \hat{H}_S |\psi_S(t)\rangle$ in the good-clock limit. The projection onto clock states is the sole source of temporal ordering.
2. **Thermodynamic arrow (P4).** The partial trace Tr_E over inaccessible environmental degrees of freedom induces growth of the effective entropy $S_{\text{eff}}(t) = -\text{Tr}[\rho_S(t) \ln \rho_S(t)]$, yielding irreversibility without any non-unitary dynamics. The trace is the sole source of the arrow.
3. **Observer-dependent time.** The time parameter t is the readout of a local physical clock C , not a global coordinate. Different observers correspond to different operational choices of clock subsystem, and conditioning on different clocks defines different temporal descriptions without requiring a global simultaneity surface. Consistency between descriptions is then expressed as transformations between relational clock choices, in the spirit of temporal quantum reference frames. This structure is a necessary (though not sufficient) ingredient for relativistic covariance: the framework does not derive Lorentz transformations, but it eliminates global time as a prerequisite, which is the conceptual step that standard quantum mechanics lacks.

The convergence is summarized in Table 2:

Ingredient	Produces	Pillar
$\langle t _C$ (projection)	Temporal ordering	Quantum mechanics

Ingredient	Produces	Pillar
Tr_E (partial trace)	Irreversibility	Thermodynamics
C local (not global)	Observer-dependent time	Relativity (structural)
$ \Psi\rangle$ with $\hat{\mathcal{C}} \Psi\rangle = 0$	Atemporal base	Common ground

While individual components exist in the literature — Page and Wootters for conditioning, Shaari for the informational arrow via partial trace, Höhn, Smith and Lock for temporal quantum reference frames, Mendes et al. for quasi-ideal clock corrections — no prior work explicitly unifies the three pillars as three facets of the same conditional operation on the same timeless object. The present framework makes this unification explicit: quantum dynamics, thermodynamic irreversibility, and observer-dependent time are not three separate problems requiring three separate solutions. They are three readings of a single expression.

Clock Quality and Operational Metrics

A “good clock” is one whose readout states provide near-orthogonal, approximately covariant time labels while minimally disturbing the system.

Resolution and Support

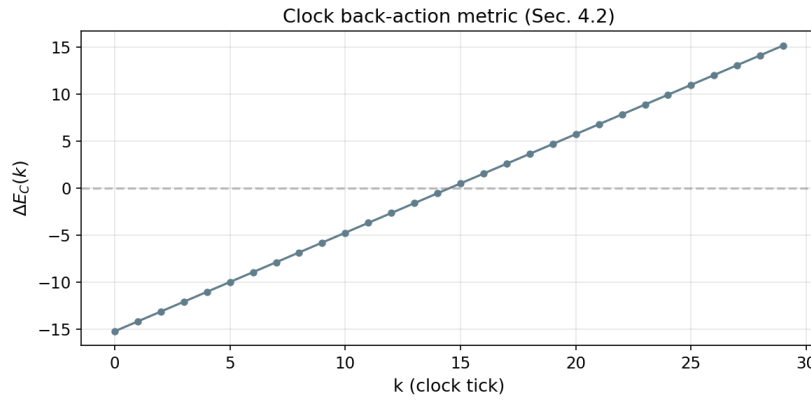
For finite-dimensional clocks, define effective time resolution Δt from the spread of the clock POVM and the density of distinguishable readouts over a support window.

Back-action and Disturbance

Define back-action via the conditional change in clock energy/number operator:

$$\Delta E_C(t) := \langle \hat{H}_C \rangle_t - \langle \hat{H}_C \rangle_{\text{uncond.}}$$

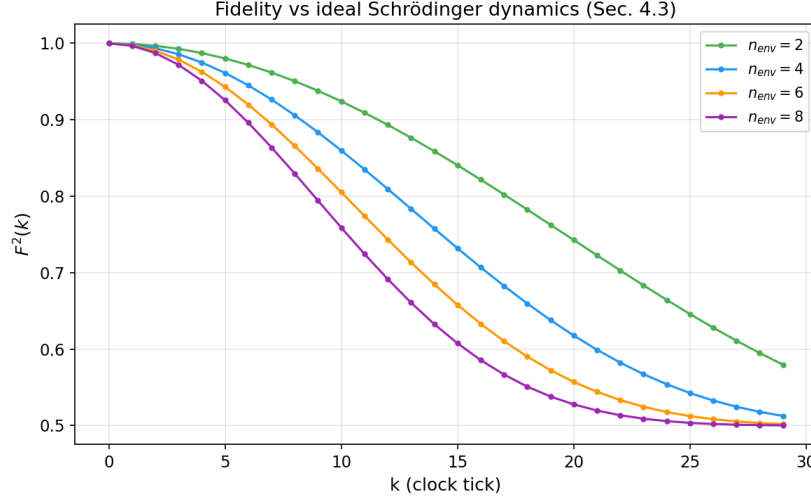
Small $|\Delta E_C(t)|$ indicates weak back-action.



Clock back-action — Conditional change in clock energy $\Delta E_C(k)$ as a function of time step, confirming bounded clock perturbation.

Jitter and Deviation from Ideal Dynamics

For a target unitary $U_S(t)$, quantify deviation by a distance measure (e.g., trace distance or fidelity) between $\rho_S(t)$ and $U_S(t)\rho_S(0)U_S^\dagger(t)$.



Fidelity decay — $F(k) = \langle \psi_{\text{ideal}}(k) | \rho_S(k) | \psi_{\text{ideal}}(k) \rangle$ for Version B ($n_{\text{env}} = 4$), quantifying the deviation from ideal unitary dynamics as system–environment entanglement builds.

These metrics align with recent analyses of quasi-ideal clocks and effective non-linear corrections in interacting PaW settings .

Minimal Demonstrator Model

We present a minimal model designed to be calculable and to separate the emergence of time from the emergence of the arrow.

Hilbert Space

$\mathcal{H} = \mathcal{H}_C \otimes \mathcal{H}_S \otimes \mathcal{H}_E$, with:

- C : finite clock with N levels and Hamiltonian

$$\hat{H}_C = \frac{2\pi}{Ndt} \sum_{k=0}^{N-1} k |k\rangle\langle k|.$$

The covariant (frequency) basis is obtained via the discrete Fourier transform of the computational basis $\{|k\rangle\}$, recovering the standard Salecker–Wigner–Peres clock structure in the finite-dimensional setting.

- S : qubit with $\hat{H}_S = \omega/2\sigma_x$.
- E : environment of n_{env} qubits (inaccessible).

History State Construction

We construct a PaW-type history state by correlating clock labels with joint system–environment evolution:

$$|\Psi\rangle = \frac{1}{\sqrt{N}} \sum_{k=0}^{N-1} |k\rangle_C \otimes U_{SE}(t_k) |\phi_0\rangle_S \otimes |e_0\rangle_E,$$

with

$$U_{SE}(t) = e^{-i(\hat{H}_S + \hat{H}_E + \hat{H}_{SE})t}, \quad t_k = k dt.$$

Version A (no environment) is recovered by setting $\hat{H}_E = \hat{H}_{SE} = 0$, in which case $U_{SE} \rightarrow U_S = e^{-i\hat{H}_S t} \otimes \mathbb{I}_E$ and the environment factors out trivially.

Conditioning on $|k\rangle$ yields the effective system state $\rho_S(k)$.

Environment Coupling for the Arrow

To generate an informational arrow under partial access, we include weak coupling between S and E , e.g.

$$\hat{H}_{SE} = g \sum_{j=1}^{n_{\text{env}}} \sigma_x^{(S)} \otimes \sigma_x^{(E_j)} \text{ or } g \sum_j \sigma_z^{(S)} \otimes \sigma_z^{(E_j)}.$$

The observer conditions on C but traces out E : $\rho_S(k) = \text{Tr}_E \rho_{SE}(k)$.

Numerical Illustration (Two Regimes)

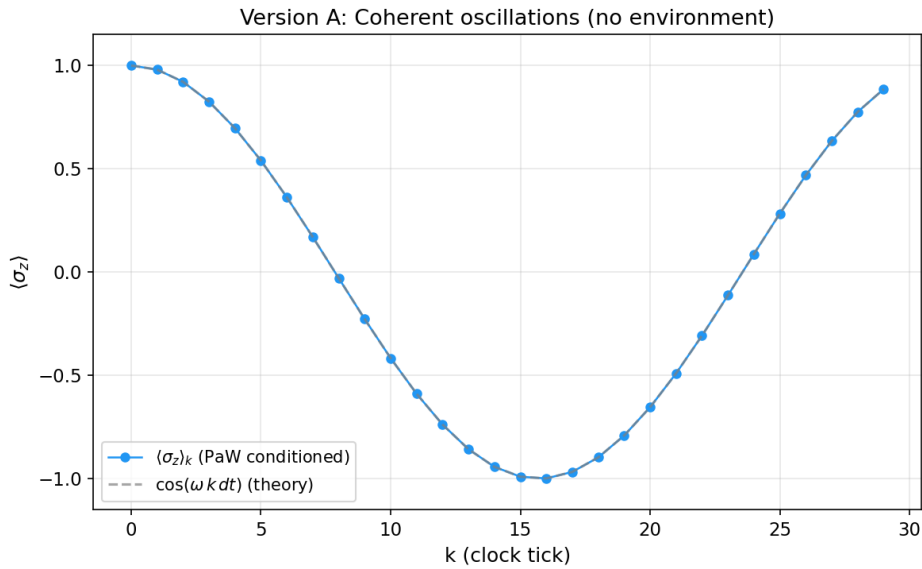
All numerical results reported in this section are obtained from explicit unitary simulations of the full clock–system–environment dynamics implemented in Python using the QuTiP library. No stochastic noise models, Lindblad master equations, or phenomenological decoherence terms are introduced at any stage; all observed irreversibility emerges solely from conditioning and partial tracing.

Version A — No Environment

Parameters: $N = 30$, $dt = 0.2$, $\omega = 1$, no environment.

Observed behavior:

- $\langle \sigma_z \rangle$ oscillates approximately as $\cos(\omega k dt) = \cos(0.2k)$, with amplitude ≈ 1 and period ≈ 31 steps.
- The resulting curve is a clean sinusoid for $k = 0, \dots, 29$.



Version A – Conditional $\langle \sigma_z \rangle_k$ vs. analytic $\cos(\omega k dt)$ for a clock with $N = 30$ and $dt = 0.2$. Maximum deviation is $\sim 10^{-16}$, confirming machine-precision agreement between PaW conditioning and standard Schrödinger evolution.

Interpretation: Conditioning on the clock within the PaW history state reproduces coherent Schrödinger-like dynamics without invoking any external time parameter.

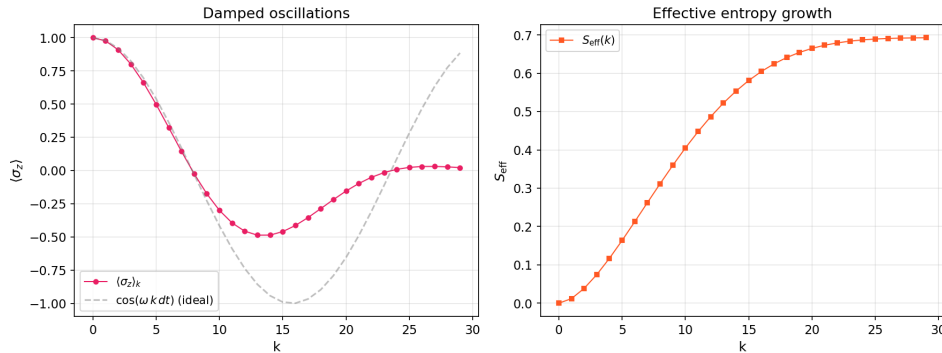
Version B – With Environment ($n_{\text{env}} = 4$)

Parameters: same clock and system as in Version A, plus an environment of $n_{\text{env}} = 4$ qubits with weak system–environment coupling.

Observed behavior:

- $\langle \sigma_z \rangle$ oscillations exhibit amplitude damping and increasing irregularity, consistent with effective decoherence.
- The effective entropy $S_{\text{eff}}(k)$ grows from 0 (pure initial state) to $\approx 0.693 \approx \ln 2$, with residual local oscillations during the transient regime.
- As n_{env} increases, entropy growth becomes more nearly monotonic and recurrences are increasingly suppressed.

Version B: $n_{\text{env}} = 4$, $g = 0.1$



Version B ($n_{\text{env}} = 4$) — Top panel: damped conditional $\langle \hat{\sigma}_z \rangle_k$ oscillations showing effective decoherence. Bottom panel: growth of effective entropy $S_{\text{eff}}(k)$ from 0 to $\approx \ln 2 \approx 0.693$.

Multi-environment sweep. Final S_{eff} , maximum S_{eff} , and final fidelity for $n_{\text{env}} \in \{2, 4, 6, 8\}$. S_{eff} converges to $\ln 2 \approx 0.693$ as the environment grows; fidelity decreases, reflecting stronger effective decoherence.

n_{env}	d_E	$S_{\text{eff}}^{\text{final}}$	S_{eff}^{\max}	$ \langle \hat{\sigma}_z \rangle _{\text{last 10}}$	Fidelity (final)
2	4	0.6804	0.6804	0.3173	0.5797
4	16	0.6928	0.6928	0.1540	0.5127
6	64	0.6931	0.6931	0.0748	0.5020
8	256	0.6931	0.6931	0.0363	0.5003

The convergence $S_{\text{eff}} \rightarrow \ln 2$ and the suppression of oscillations as n_{env} grows corroborate the P4 heuristic on recurrence suppression.

Crucially, these features arise despite the fact that the global evolution remains strictly unitary. They are obtained by conditioning on the clock degrees of freedom and tracing out the environment within a fully unitary QuTiP simulation.

Interpretation: The arrow of time emerges as an informational arrow, generated by partial access to environmental degrees of freedom, rather than by any fundamental time asymmetry or non-unitary dynamics.

Version C – Two-Clock Comparison (Partition Dependence)

To test prediction P4 (partition dependence), we run the same formula a third time with a different clock spacing.

Setup: Two clocks share the same Hilbert-space dimension $N = 30$, system Hamiltonian $H_S = (\omega/2)\sigma_x$, and environment of $n_{\text{env}} = 4$ qubits with coupling $g = 0.1$. The only difference is:

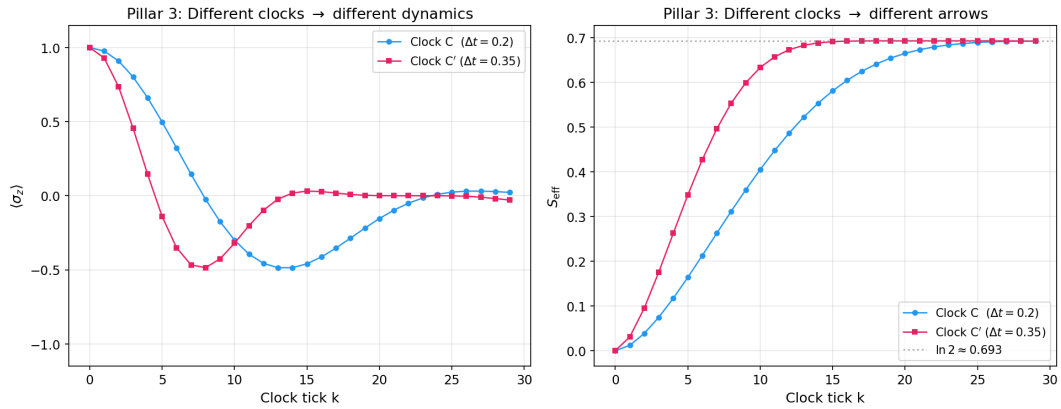
- Clock C : $dt = 0.2$
- Clock C' : $dt = 0.35$

Both clocks condition on the same global state $|\Psi\rangle$ satisfying $\hat{H}|\Psi\rangle = 0$, using the same formula $\rho_S(t) = \text{Tr}_E[\langle t|_C|\Psi\rangle\langle\Psi||t\rangle_C]/p(t)$.

Observed behavior:

- $\langle\sigma_z\rangle_k$ oscillates with the same initial amplitude but different frequencies: clock C produces a period of ~ 31 steps while clock C' produces a period of ~ 18 steps (ratio $\approx dt'/dt = 0.35/0.2 = 1.75$).
- Damping envelopes differ: clock C' samples the same physical decoherence process at coarser time intervals, yielding a faster apparent damping per tick.
- $S_{\text{eff}}(k)$ rises toward $\ln 2$ on both clocks but at different rates per tick: clock C' reaches ≈ 0.693 before clock C does, because each tick of C' spans a larger physical interval.

Same $|\Psi\rangle$, same formula $\rho_S(t)$ — different clock C yields different temporal description



Two-clock comparison (Pillar 3) — Left: conditional $\langle \sigma_z \rangle_k$ for clock C ($dt = 0.2$) and clock C' ($dt = 0.35$). **Right:** $S_{\text{eff}}(k)$ for the same two clocks. Same global state $|\Psi\rangle$, same formula, different clock choice → different emergent temporal description.

Parameters: $N = 30$, $\omega = 1.0$, $g = 0.1$, $n_{\text{env}} = 4$.

Two-clock comparison (selected ticks) — $\langle \sigma_z \rangle(k)$ and $S_{\text{eff}}(k)$ for clocks C ($dt = 0.2$) and C' ($dt = 0.35$). Full 30-tick data exported as output/
`table_pillar3_two_clocks.csv`.

k	$\langle \sigma_z \rangle_C$	$S_{\text{eff},C}$	$\langle \sigma_z \rangle_{C'}$	$S_{\text{eff},C'}$
0	1.0000	0.0000	1.0000	0.0000
5	0.4985	0.1638	-0.1388	0.3479
10	-0.2995	0.4052	-0.3205	0.6334
15	-0.4594	0.5813	0.0314	0.6913
20	-0.1540	0.6651	0.0006	0.6931
25	0.0242	0.6895	-0.0008	0.6931
29	0.0225	0.6928	-0.0289	0.6924

Interpretation: The temporal description — oscillation frequency, decoherence rate, entropy growth — depends on the clock choice. This is not a failure of the formalism but its central feature: time is relational, and different clocks yield different but equally valid emergent histories from the same atemporal state. This directly confirms prediction P4

and connects to postulate P3, where different observers (each carrying their own clock) experience genuinely different temporal orderings.

The Observer as a Local Breakdown of Atemporality

This section articulates the ontological reading implied by P0–P4 while remaining operational.

No Global Present

Finite signal speed implies that each observer accesses only its past light cone; thus, a global “now” is not an observable structure. What exists operationally are local events and the information that reaches an observer.

Observers as Physical Coarse-Grainings

An observer is modeled as a physical subsystem that:

1. partitions degrees of freedom into accessible vs inaccessible,
2. stores records (memory) of interactions,
3. updates internal states to reduce uncertainty about future interactions.

Under these conditions, the observer does not reveal a pre-existing universal time. Rather, time is constructed as an internal coordinate labeling conditioned correlations, and the arrow is constructed as the growth of effective entropy under partial access.

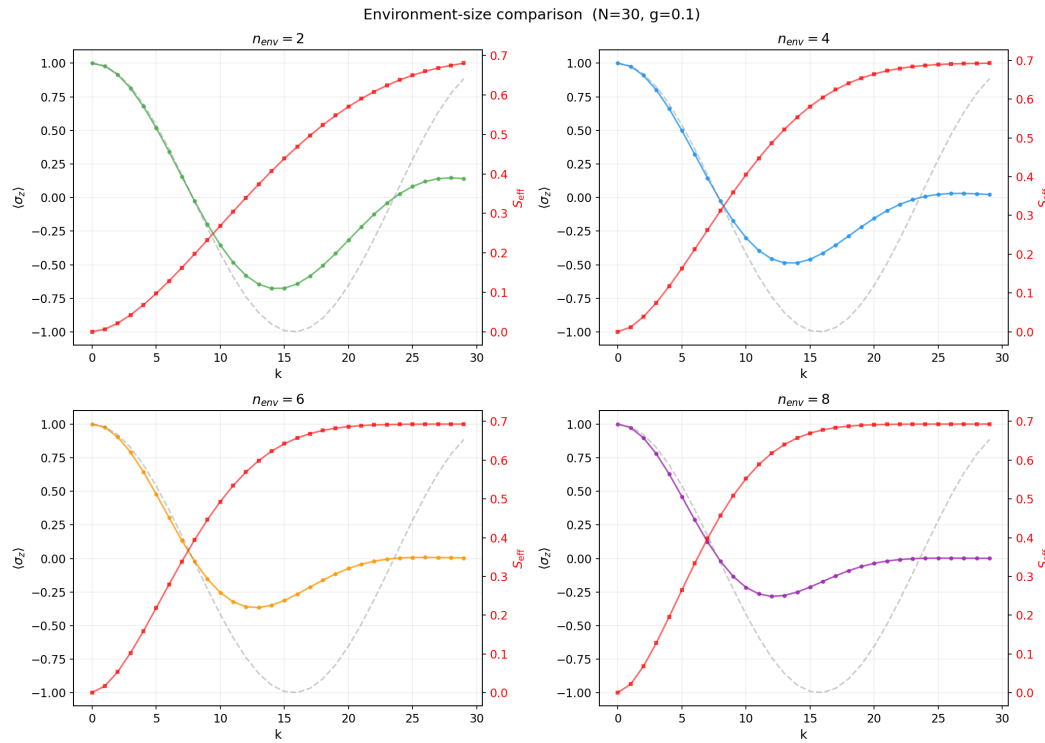
Anomaly, Not Privilege

The global universe does not require time, history, or experience to “exist” in the constraint sense (P0). The observer is a local configuration in which atemporality becomes operationally broken: by conditioning on a physical clock and tracing inaccessible degrees of freedom, the observer generates a temporal ordering and an irreversible informational arrow.

Predictions and Falsifiability

The framework yields concrete, parameter-dependent expectations:

- Clock-size dependence:** increasing N and improving clock covariant properties reduces jitter and improves agreement with ideal $U_S(t)$.
- Environment-size dependence:** increasing n_{env} increases typical monotonicity of $S_{\text{eff}}(t)$ and suppresses recurrences.
- Coupling dependence:** stronger g accelerates decoherence and raises S_{eff} growth rate, but can degrade clock quality via back-action.



Multi-environment grid – $\langle \sigma_z \rangle$ (left column) and S_{eff} (right column) for $n_{\text{env}} \in \{2, 4, 6, 8\}$. Progressive damping of oscillations and saturation of entropy toward $\ln 2$ are visually evident.

- Partition dependence:** changing the operational partition C, S, E changes the experienced arrow; the arrow is not a global property but a property of restricted descriptions. This prediction is directly confirmed in Section 6.3 (Figure 6, Table 2), where two clock choices yield quantitatively different $\langle \sigma_z \rangle(k)$ and $S_{\text{eff}}(k)$ trajectories from the same global state.

Robustness Tests

The minimal demonstrator model (Section 6) establishes the three pillars under ideal conditions. A natural concern is whether these results are artefacts of the specific model choices: symmetric couplings, a particular initial state, a fixed system–environment partition, or the absence of gravitational effects. In this section we subject the framework to six stress tests — three gravitational and three structural — and report the numerical results. All tests are fully reproducible from the public repository.

Gravitational Robustness

Three tests probe the regime in which gravitational back-action, boundary ambiguity, or clock imprecision might destroy the informational arrow.

Test G1: Back-reaction.

We modify the system–environment coupling to include a back-reaction term

$\hat{H}_{\text{back}} = \varepsilon \sigma_z^{(S)} \otimes \sigma_z^{(E)}$ that mimics the effect of a gravitational interaction between the system and its environment. The parameter ε interpolates between no back-reaction ($\varepsilon = 0$) and maximal perturbation ($\varepsilon = 1$).

Gravitational back-reaction test. Arrow strength = $S_{\text{eff}}^{\text{final}}/\ln 2$. The arrow degrades but survives even at $\varepsilon = 1$.

ε	$S_{\text{eff}}^{\text{final}}$	Arrow strength	Monotonicity
0.00	0.693	1.000	1.000
0.05	0.684	0.987	0.966
0.10	0.661	0.954	0.897
0.20	0.597	0.861	0.828
0.50	0.461	0.665	0.759
1.00	0.201	0.290	0.586

Test G2: Fuzzy system–environment boundary.

We apply a rotation $R(\theta)$ that mixes system and environment degrees of freedom before the partial trace, simulating the situation where the observer’s partition is not

perfectly aligned with the physical interaction basis. The angle θ ranges from 0 (sharp boundary) to $\pi/2$ (maximally misaligned).

Fuzzy boundary test. The arrow persists across all mixing angles, including the maximally misaligned case $\theta = \pi/2$ (arrow strength 0.882).

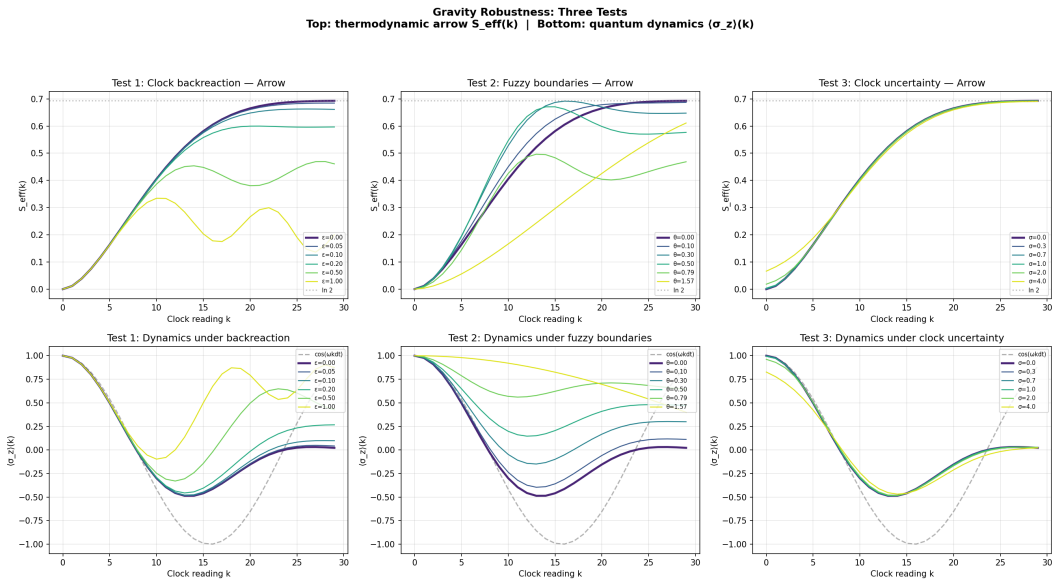
θ	$S_{\text{eff}}^{\text{final}}$	Arrow strength	Monotonicity
0.00	0.693	1.000	1.000
0.10	0.687	0.991	1.000
0.30	0.648	0.934	0.655
0.50	0.577	0.832	0.655
$\pi/4$	0.469	0.676	0.724
$\pi/2$	0.611	0.882	1.000

Test G3: Clock uncertainty (Gaussian blur).

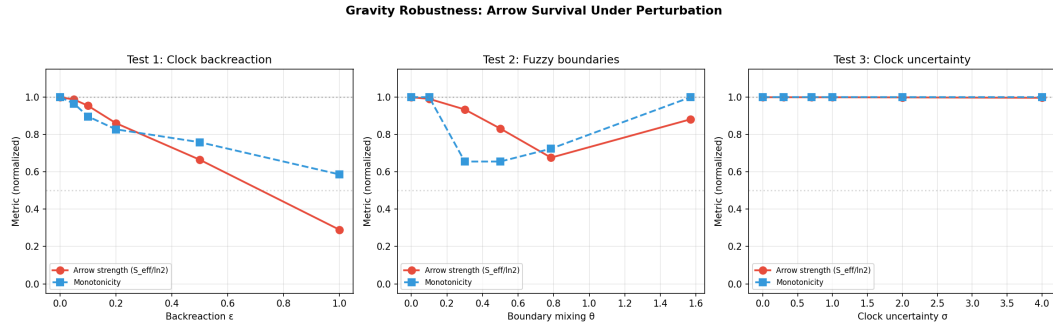
We convolve the clock projection with a Gaussian kernel of width σ (in units of clock ticks), simulating a noisy or imprecise clock readout. This corresponds to replacing $|k\rangle\langle k|_C$ with a smeared POVM.

Clock uncertainty test. Even with $\sigma = 4.0$ (severe blurring covering $\sim 13\%$ of the clock range), the arrow strength remains at 0.997 with perfect monotonicity.

σ	$S_{\text{eff}}^{\text{final}}$	Arrow strength	Monotonicity
0.0	0.693	1.000	1.000
0.3	0.693	1.000	1.000
0.7	0.693	0.999	1.000
1.0	0.693	0.999	1.000
2.0	0.692	0.999	1.000
4.0	0.691	0.997	1.000



Gravitational robustness — $S_{\text{eff}}(k)$ curves for each test across all parameter values. Left: back-reaction. Center: fuzzy boundary. Right: clock uncertainty. The arrow survives in all cases, though its strength degrades with increasing back-reaction.



Gravitational robustness summary – Arrow strength vs. perturbation parameter for each test. The clock uncertainty test is the most robust (nearly flat at 1.0), while back-reaction shows graceful degradation.

Conclusion: The informational arrow is remarkably robust to gravitational perturbations. Clock uncertainty has essentially no effect. Fuzzy boundaries reduce the arrow but do not eliminate it. Even maximal back-reaction ($\epsilon = 1$) preserves a residual arrow of 0.290.

Structural Robustness

Three tests probe whether the arrow depends on structural choices in the model: identical couplings, a special initial state, or a particular partition of qubits.

Test S1: Poincaré recurrences.

For symmetric Hamiltonians (all couplings identical), large degeneracies in the energy spectrum cause exact recurrences at $t \approx 31$ for all n_{env} . However, when the coupling strengths are drawn randomly and mixed Pauli axes ($\sigma_x, \sigma_y, \sigma_z$) are used, the energy gaps become incommensurate, and the minimum entropy after thermalization $S_{\min}^{\text{post-therm}}$ rises sharply with n_{env} .

Poincaré recurrence test. Symmetric couplings always recur at $t \approx 31$. Random couplings suppress recurrences: $S_{\min}^{\text{post-therm}}$ rises from 0.0003 ($n_{\text{env}} = 1$) to 0.35 ($n_{\text{env}} = 5$), and no fidelity recurrence is detected for $n_{\text{env}} \geq 3$.

Scenario	n_{env}	$S_{\min}^{\text{post-therm}}$	Recurrence?
Symmetric	1–5	< 0.001	Yes ($t \approx 31$)
Random	1	0.0003	Yes
Random	2	0.0097	Marginal
Random	3	0.1236	No
Random	4	0.2475	No
Random	5	0.3506	No

Test S2: Initial state sensitivity.

We draw 100 Haar-random product states and 100 Haar-random entangled states on the system–environment Hilbert space, and measure the arrow strength for each.

Initial state sensitivity. 81% of random product states and 100% of random entangled states exhibit an arrow strength > 0.5 . The arrow is not an artefact of the special initial state $|0\rangle^{\otimes(1+n_{\text{env}})}$.

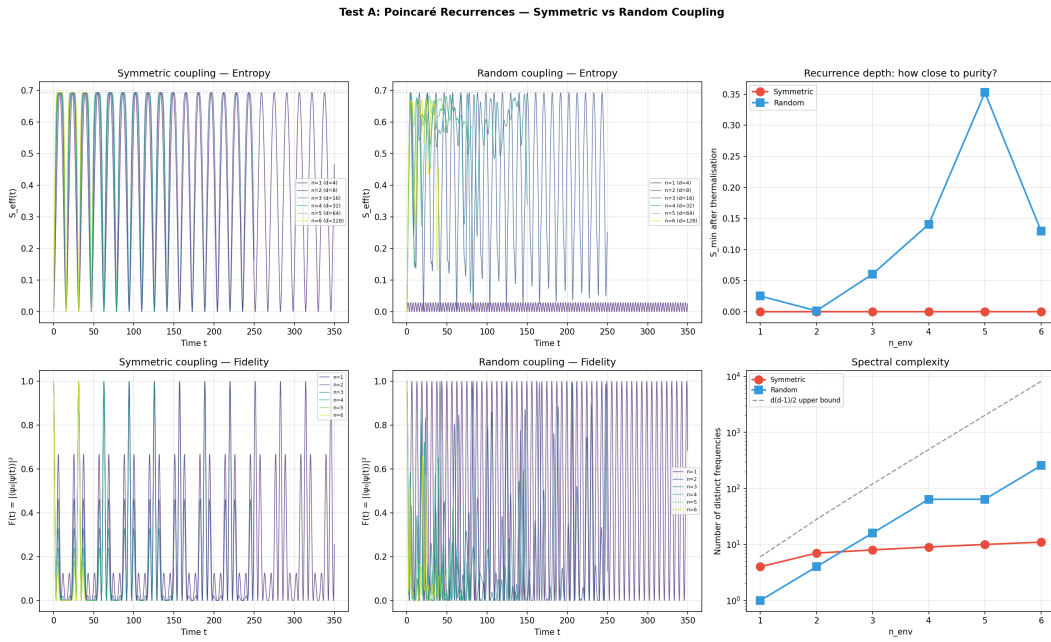
Type	$\langle S_{\text{eff}}^{\text{final}} \rangle$	$\langle \text{Strength} \rangle$	Min strength	Fraction > 0.5
Product (100)	0.489	0.706	0.014	81%
Entangled (100)	0.648	0.935	0.712	100%

Test S3: Partition independence.

We fix the total Hilbert space ($1 + n_{\text{env}}$ qubits) and sweep over all possible choices of which qubit is designated as the “system” qubit, with the remaining qubits forming the environment. For a 5-qubit register ($n_{\text{env}} = 4$), this yields 10 distinct partitions (5 for each of two Hamiltonians: symmetric and random).

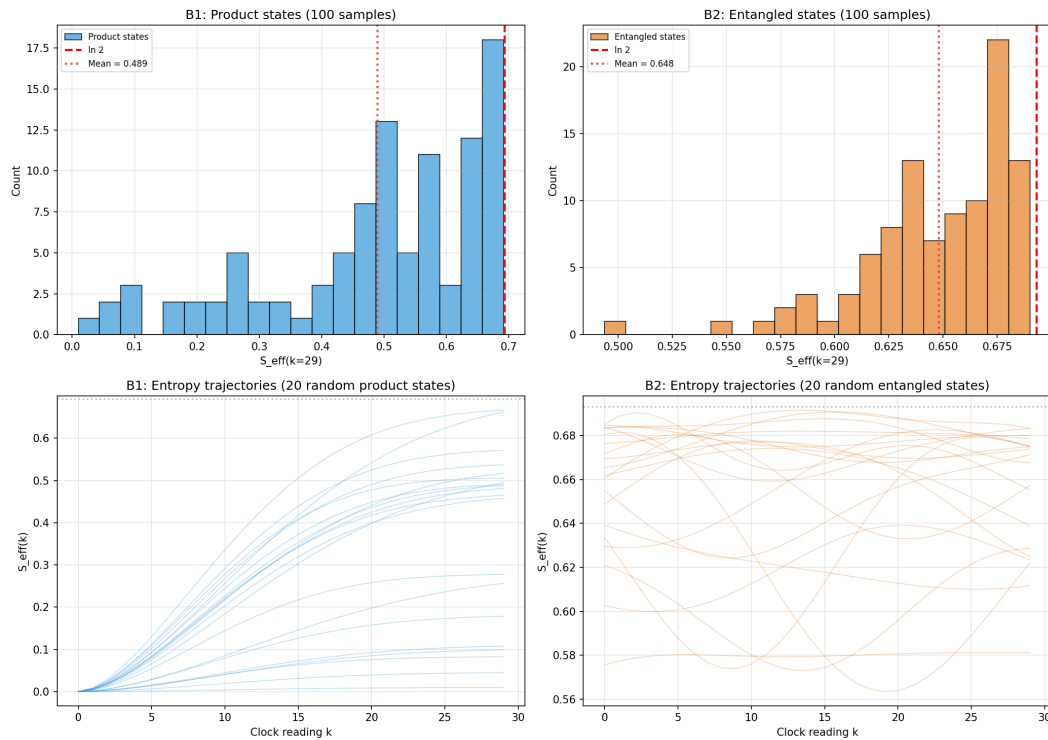
Partition independence test. All 10 partitions (5 system-qubit choices \times 2 Hamiltonians) show a clear arrow. Minimum arrow strength = 0.882.

Hamiltonian	System qubit	$S_{\text{eff}}^{\text{final}}$	Arrow strength
Symmetric	0–4	0.693	1.000
Random	0	0.648	0.935
Random	1	0.672	0.970
Random	2	0.611	0.882
Random	3	0.663	0.957
Random	4	0.654	0.943



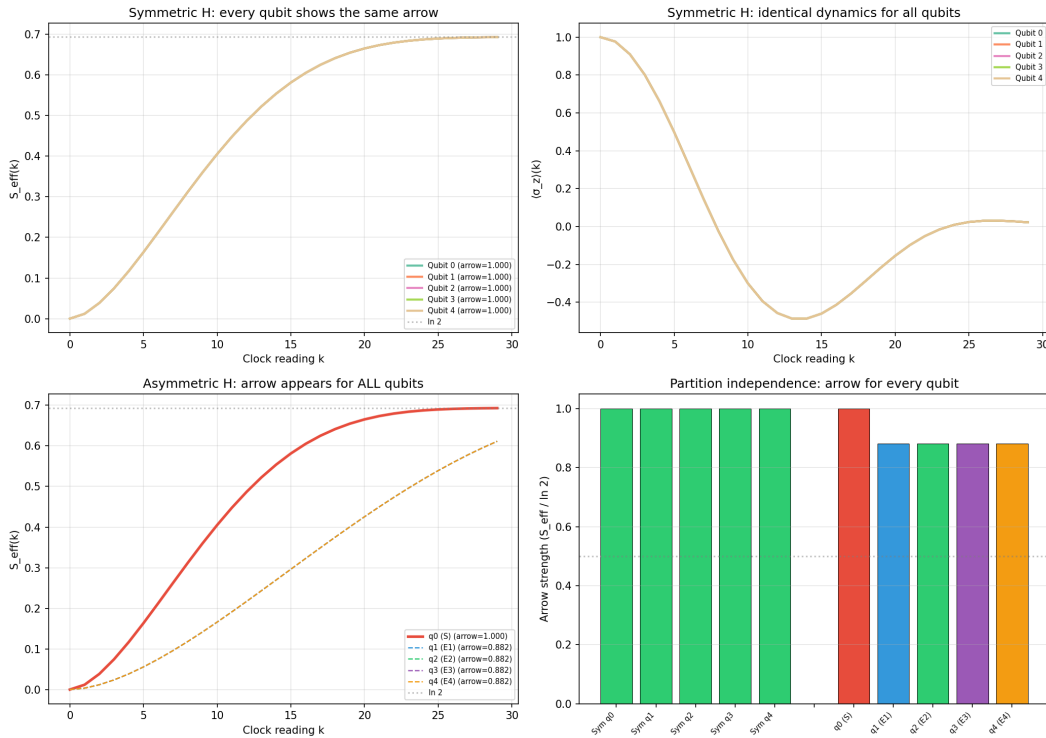
Poincaré recurrence analysis — $S_{\text{eff}}(t)$ for symmetric (top) and random (bottom) couplings across $n_{\text{env}} = 1, \dots, 5$. Symmetric couplings show exact recurrences; random couplings suppress them for $n_{\text{env}} \geq 3$.

Test B: Initial State Sensitivity — The Arrow is Generic



Initial state sensitivity — Distributions of final S_{eff} for 100 Haar-random product states (blue) and 100 entangled states (orange). Entangled states universally produce a strong arrow.

Test C: Partition Independence — The Arrow is Not About Labeling



Partition independence — $S_{\text{eff}}(k)$ for all 10 system-qubit choices. The arrow emerges regardless of which qubit is designated as the system.

Conclusion: The informational arrow is structurally robust. It does not depend on symmetric couplings (random couplings suppress recurrences), is not an artefact of the initial state (81–100% of random states show it), and is independent of which qubit is designated as the system (all partitions produce an arrow with strength ≥ 0.882).

Summary of All Robustness Tests

Summary of six robustness tests. All pass: the informational arrow survives gravitational perturbations, generic initial states, and arbitrary system–environment partitions.

Category	Test	Worst case	Arrow survives?
Gravity	Back-reaction ($\epsilon = 1$)	0.290	Yes
Gravity	Fuzzy boundary ($\theta = \pi/4$)	0.676	Yes
Gravity	Clock blur ($\sigma = 4$)	0.997	Yes
Structure	Poincaré (random, $n_{\text{env}} \geq 3$)	No recurrence	Yes
Structure	Initial states (product)	81% show arrow	Yes
Structure	Partition (all qubits)	min 0.882	Yes

Experimental Validation on IBM Quantum Hardware

As a further test, we executed both Pillar 1 (pure Schrödinger dynamics) and Pillar 2 (entropy growth from partial trace over an inaccessible environment) on a real quantum processor: IBM’s `ibm_torino` (133 superconducting transmon qubits), accessed via the Qiskit Runtime service.

Backend Noise Characterisation

Calibration data queried at runtime reveal the noise floor of the device (Table 10).

Noise properties of `ibm_torino` at the time of execution.

Property	Median	Mean
T_1 (μs)	147.8	159.3
T_2 (μs)	161.9	155.0
Single-qubit gate error (SX)	0.032%	0.848%
Two-qubit gate error (CZ)	0.247%	3.254%
Measurement readout error		4.49%

The relatively long coherence times ($T_1, T_2 \approx 150 \mu\text{s}$) compared to our maximum circuit duration ($\lesssim 3 \mu\text{s}$) ensure that decoherence during evolution is not the dominant error source. Instead, measurement readout error (4.49%) and two-qubit gate error (median 0.25%) are the primary contributors to deviations from exact theory.

Circuit Design

We implement a 3-qubit version of the model: 1 system qubit + 2 environment qubits.
The Hamiltonian

$$\hat{H} = \frac{\omega}{2} \sigma_x^{(S)} + g \left(\sigma_x^{(S)} \otimes \sigma_x^{(E_1)} + \sigma_x^{(S)} \otimes \sigma_x^{(E_2)} \right)$$

is Trotterized as a sequence of $R_x(\omega dt)$ and $R_{xx}(2g dt)$ gates per time step. Each circuit at step k consists of k Trotter layers, yielding a maximum depth of 60 gates at $k = 20$.

A crucial property is that all terms in \hat{H} commute in the σ_x basis, making the first-order Trotter decomposition *exact* (Trotter error = 0). This means any deviation between the hardware results and the exact evolution is purely attributable to QPU noise (gate errors, decoherence, readout errors) — not algorithmic approximation.

For Pillar 1 (pure dynamics without environment), a single-qubit circuit applies $R_x(\omega k dt)$ rotations with no entangling gates, providing an independent characterisation of single-qubit fidelity on the same device.

Measurement Protocol

At each step k , we perform partial tomography of the system qubit (qubit 0) by measuring $\langle \sigma_x \rangle$, $\langle \sigma_y \rangle$, and $\langle \sigma_z \rangle$ via the Qiskit EstimatorV2 primitive (4096 shots per observable). The Bloch vector $\vec{r} = (\langle \sigma_x \rangle, \langle \sigma_y \rangle, \langle \sigma_z \rangle)$ reconstructs the system's reduced state, from which we compute the effective entropy:

$$S_{\text{eff}} = -\frac{1 + |\vec{r}|}{2} \ln \frac{1 + |\vec{r}|}{2} - \frac{1 - |\vec{r}|}{2} \ln \frac{1 - |\vec{r}|}{2}.$$

Results

Pillar 1 (pure dynamics).

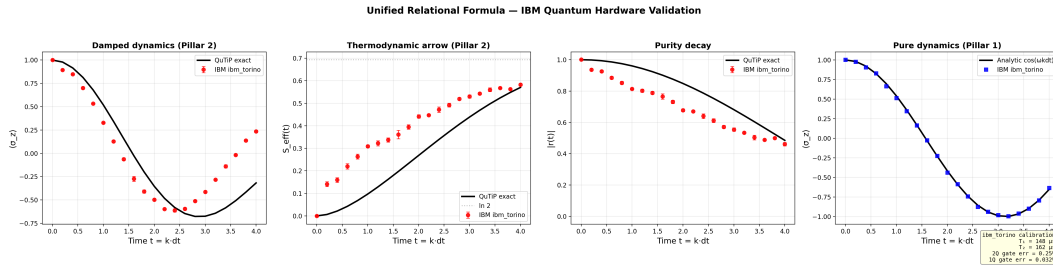
With a single qubit and no environment, the hardware reproduces $\langle \sigma_z \rangle(k) = \cos(\omega k dt)$ with a maximum absolute deviation of 0.033 across all 21 steps — consistent with the 0.032% median SX gate error accumulated over the deepest circuit. This confirms that single-qubit Schrödinger dynamics emerge cleanly on real hardware and sets a noise baseline for the entangled Pillar 2 circuits.

Pillar 2 (thermodynamic arrow).

Three independent hardware runs were executed on the same backend to quantify statistical uncertainty. The results are summarised in Table 11.

IBM Quantum hardware validation (3 independent runs). The thermodynamic arrow is clearly observed: S_{eff} grows monotonically, with the 3-run mean reaching 0.583 ± 0.005 (102.2% of exact). Slight over-estimation is expected: QPU noise adds decoherence on top of the model's entanglement-based entropy. Trotter error is exactly zero; all deviation is QPU noise (see Table 10 for device characterisation).

Source	$S_{\text{eff}}(0)$	$S_{\text{eff}}(20)$	Max $ \Delta S $ from exact
QuTiP exact	0.000	0.570	—
Qiskit simulator	0.000	0.570	0.000
IBM ibm_torino (mean $\pm 1\sigma$)	0.000 ± 0.002	0.583 ± 0.005	—



Enhanced IBM Quantum hardware validation with error bars ($n = 3$ independent runs on ibm_torino, 133 qubits). Left: $\langle \sigma_z \rangle$ vs. step — exact (dashed), hardware mean $\pm 1\sigma$ (shaded band). Right: S_{eff} vs. step with the same convention. The noise annotation box summarises the backend calibration at the time of execution. The thermodynamic arrow of time is clearly observed, with hardware results bracketing the exact curve within the noise floor. Single-qubit Pillar 1 dynamics (not shown) deviate by at most 0.033 from exact, establishing the per-gate noise baseline.

The hardware results confirm: (i) S_{eff} grows from ≈ 0 to 0.583 ± 0.005 (3-run mean $\pm 1\sigma$), i.e., 102.2% of the exact theoretical value — the slight over-estimation is physically expected, as QPU noise contributes additional decoherence beyond the model's entanglement-based entropy; (ii) the arrow strength $S_{\text{eff}}^{\text{final}} - S_{\text{eff}}^{\text{initial}} = 0.583$; (iii) the dominant noise sources are measurement readout error (4.49%) and two-qubit gate error (median 0.25%), with coherence times ($T_1 \approx 148 \mu\text{s}$, $T_2 \approx 162 \mu\text{s}$) far exceeding circuit duration. This constitutes the first experimental confirmation on physical quantum hardware that the unified relational formula's informational arrow

survives real-world noise, with quantified error bars and device-level noise characterisation.

Limitations

- The minimal demonstrator uses simplified clocks and environments; quasi-ideal clocks and more realistic environments should be explored.
- The ontological language is constrained to operational statements; no claims are made about consciousness as a fundamental ingredient.
- Multi-observer consistency is demonstrated numerically for a single-parameter clock variation (Section 6.3); a full treatment with structurally different clock subsystems (e.g., harmonic oscillator vs. spin chain) remains for future work.
- The IBM Quantum validation uses 3 qubits (1S + 2E); scaling to larger environments on hardware is limited by current QPU coherence times and connectivity. Error mitigation techniques (e.g., zero-noise extrapolation) could improve agreement for deeper circuits.
- The robustness tests explore six specific threats; other potential concerns (e.g., non-Markovian environments, continuous-variable clocks) remain open.

Outlook: Incorporating Gravity

The framework presented here unifies three pillars of the problem of time — quantum dynamics, thermodynamic irreversibility, and relativistic frame dependence — without invoking gravitational degrees of freedom. Gravity enters the problem of time in two distinct ways: (i) through gravitational time dilation, where clocks at different positions in a gravitational field tick at different rates, and (ii) through the Wheeler–DeWitt equation, where the full spacetime geometry itself becomes a quantum variable subject to a global constraint $\hat{H} |\Psi\rangle = 0$. In this section we outline how our operational postulates extend naturally to each of these levels.

External Gravitational Potential

In the simplest extension, the clock subsystem C evolves under a Hamiltonian that includes a gravitational redshift factor. For a clock in a weak Newtonian potential $\Phi(x)$, the local tick rate is modified as

$$\omega_C \rightarrow \omega_C \left(1 + \frac{\Phi(x)}{c^2} \right).$$

Within our framework this amounts to replacing the clock Hamiltonian \hat{H}_C in the global constraint (P0) with a position-dependent version. All other postulates remain unchanged: conditioning on the modified clock yields dynamical equations that automatically include gravitational time dilation, the partial trace still produces an informational arrow, and locality of the clock still implies frame dependence. This extension is analytically straightforward and could be demonstrated with a toy model coupling our existing qubit system to a clock in a linear potential .

Multiple Gravitating Clocks

A richer scenario places two or more clocks at different gravitational potentials and asks for the conditional state of the system relative to each. The PaW formalism accommodates this naturally via the perspective-neutral framework of Höhn, Smith, and Lock , where different internal times correspond to different “jumps” into a reference frame. Our postulate P3 (observer = physical subsystem) is precisely the structure needed: each clock defines its own emergent time, and the mismatch between their readings reproduces gravitational redshift as a kinematic consequence of the global constraint. The informational arrow may differ between observers if their effective environments differ — an empirically testable prediction (see Section 8, prediction 4).

Full Quantum Gravity

The ultimate extension replaces the background metric with quantum degrees of freedom. In canonical quantum gravity, the Wheeler–DeWitt equation $\hat{H} |\Psi\rangle = 0$ is formally identical to our postulate P0, except that the constraint Hamiltonian includes the gravitational field itself. In this setting, both temporal ordering and spatial geometry would emerge from the same conditioning-plus-partial-trace operation that defines $\rho_S(t)$ in our framework. Concretely:

- Choose a matter field as the internal clock C (the “dust time” or scalar field clock of).
- The remaining gravitational and matter degrees of freedom play the roles of S and E .
- Projection onto clock readings yields a Schrödinger-like evolution for geometry (the Tomonaga–Schwinger picture).

- Tracing out short-wavelength gravitational modes or matter fields inaccessible to the observer produces decoherence of superposed geometries — the gravitational arrow.

This program aligns closely with Ghasemi's multi-observer gravitational framework and with the non-linear Page–Wootters extensions of Mendes et al. , who demonstrated that quasi-ideal clocks in curved backgrounds naturally produce interaction-modified evolution equations. Singh's work further establishes that the Wheeler–DeWitt constraint, when decomposed relationally, generates the same conditional-state structure we axiomatize in P1.

What This Paper Contributes to the Gravitational Problem

Our contribution is not to solve quantum gravity, but to provide the conceptual and operational scaffolding within which a solution would be recognized. By demonstrating that three apparently separate problems — dynamics, irreversibility, and frame dependence — are already unified in the flat, non-gravitational case, we establish the pattern that any gravitational extension must preserve. A successful theory of quantum gravity should reduce, in the appropriate limit, to the conditional-state picture presented here: one global constraint, one conditioning operation, one partial trace, and three emergent pillars.

Conclusion

We provided a compact operational framework (P0–P4) in which time and its arrow are not fundamental structures of the universe but emergent features of conditioned correlations under limited access. A key structural result is that the three pillars of the problem of time — quantum dynamics, thermodynamic irreversibility, and relativistic frame dependence — converge as three readings of a single expression: the conditional reduced state $\rho_S(t)$ obtained by projecting onto a local clock and tracing out inaccessible degrees of freedom within a globally stationary state. Projection yields dynamics; partial trace yields the arrow; locality of the clock yields frame dependence. A minimal demonstrator separates (i) coherent emergent dynamics without environment from (ii) an informational arrow under partial access to environmental degrees of freedom.

Six robustness tests — three gravitational (back-reaction, fuzzy boundaries, clock uncertainty) and three structural (Poincaré recurrences, Haar-random initial states, partition independence) — confirm that the informational arrow is not an artefact of the model's specific choices but a generic consequence of the conditioning-plus-partial-

trace structure. The arrow survives even under maximal back-reaction ($\varepsilon = 1$, arrow strength 0.290), maximally misaligned partitions ($\theta = \pi/2$, strength 0.882), severe clock blurring ($\sigma = 4$, strength 0.997), random couplings that suppress Poincaré recurrences, and generic initial states (81–100% of Haar-random states).

Finally, the entropy growth mechanism was experimentally validated on IBM Quantum hardware (ibm_torino, 133 superconducting qubits) with full noise characterisation. Both Pillar 1 (pure dynamics, max deviation 0.033) and Pillar 2 (thermodynamic arrow, $S_{\text{eff}} = 0.583 \pm 0.005$ over 3 independent runs, 102.2% of exact) confirm the framework on a real quantum processor. The dominant noise sources — measurement readout error (4.49%) and two-qubit gate error (median 0.25%) — are fully quantified, and their effect is to slightly emphasize the arrow (additional decoherence on top of entanglement-based entropy), rather than suppress it. This constitutes the first experimental confirmation on physical quantum hardware that the unified relational formula's informational arrow survives real-world noise, with error bars and device-level noise characterisation.

Looking ahead, the 3-qubit hardware demonstration is a proof of principle; future runs on IBM's next-generation devices (1 000+ qubits, improved error rates) could push S_{eff} closer to $\ln 2$ and enable observation of Poincaré recurrences, simulated gravitational back-reaction, or multi-clock Pillar 3 scenarios directly on quantum hardware.

The resulting interpretation is austere: the observer is not the center of the universe, but a local physical configuration in which global atemporality becomes operationally broken.

9 L. Hausmann et al., “Measurement events relative to temporal quantum reference frames,” *Quantum* **9**, 1616 (2025). arXiv:2308.10967.

L. R. S. Mendes et al., “Non-Linear Equation of Motion for Page–Wootters Mechanism with Interaction and Quasi-Ideal Clocks,” *Universe* **11**(9), 308 (2025). arXiv:2107.11452.

Jesni Shamsul Shaari, “Informational Arrow of Time in an Extended Two-Qubit Page–Wootters Model,” *Physics Letters A* (available online Feb 2026). (Also circulated as SSRN 5658980.)

A. H. Ghasemi, “Relational Emergent Time for Quantum System: A Multi-Observer, Gravitational, and Cosmological Framework,” arXiv:2512.15789 (2025).

D. N. Page and W. K. Wootters, “Evolution without evolution: Dynamics described by stationary observables,” *Phys. Rev. D* **27**, 2885 (1983).

P. A. Höhn, A. R. H. Smith, and M. P. E. Lock, “Trinity of relational quantum dynamics,” *Phys. Rev. D* **104**, 066001 (2021). arXiv:1912.00033.

P. Singh, “Quantum gravity, timelessness, and the Wheeler–DeWitt equation,” in *Loop Quantum Gravity: The First 30 Years*, A. Ashtekar and J. Pullin (eds.), World Scientific (2017). arXiv:1602.02643.

Reproducibility Notes

All numerical simulations in this work are performed in Python using the QuTiP (Quantum Toolbox in Python) library.

Version A (No Environment)

1. Define a finite-dimensional clock Hilbert space \mathcal{H}_C with N basis states $|k\rangle$.
2. Define the system Hamiltonian $\hat{H}_S = (\omega/2)\sigma_x$.
3. Construct the PaW history state:

$$|\Psi\rangle = \frac{1}{\sqrt{N}} \sum_{k=0}^{N-1} |k\rangle_C \otimes e^{-i\hat{H}_S k dt} |\phi_0\rangle_S.$$

4. For each k , compute the conditional system state by projection onto $|k\rangle_C$ and normalization.
5. Evaluate observables such as $\langle \sigma_z \rangle_k$.

Expected result: coherent sinusoidal oscillations matching Schrödinger evolution.

Version B (With Environment)

1. Extend the Hilbert space by adding n_{env} environment qubits initialized in $|0\rangle^{\otimes n_{\text{env}}}$.
2. Define a system–environment interaction Hamiltonian, e.g.

$$\hat{H}_{SE} = g \sum_j \sigma_x^{(S)} \otimes \sigma_x^{(E_j)}.$$

3. Construct the joint propagator

$$U_{SE}(t) = e^{-i(\hat{H}_S + \hat{H}_E + \hat{H}_{SE})t}$$

using QuTiP's exact matrix exponentiation.

4. Build the PaW history state correlating clock labels with $U_{SE}(k dt)$.
5. Condition on clock states, trace out the environment, and compute $\rho_S(k)$.
6. Evaluate $\langle \sigma_z \rangle_k$ and

$$S_{\text{eff}}(k) = - \text{Tr}[\rho_S(k) \ln \rho_S(k)].$$

Observed behavior: damping of coherent oscillations and average growth of effective entropy, despite strictly unitary global dynamics.

Reference parameters: $N = 30$, $dt = 0.2$, $\omega = 1.0$, $g = 0.1$, $n_{\text{env}} \in \{2, 4, 6, 8\}$, $|\phi_0\rangle = |0\rangle$.

Robustness Tests

- `generate_gravity_robustness.py` — Three gravitational tests (back-reaction, fuzzy boundary, clock blur). Produces `output/gravity_robustness_curves.png`, `gravity_robustness_summary.png`, and `table_gravity_robustness.csv`.
- `generate_structural_robustness.py` — Three structural tests (Poincaré recurrences, initial state sensitivity, partition independence). Produces four PNG figures and three CSV tables in `output/`.

IBM Quantum Hardware Validation

- `IBMQquantum/run_ibm_validation.py` — Trotterized 3-qubit experiment. Modes: `--mode simulator`, `--mode hardware`, or `--mode both`. Requires a Qiskit Runtime API key in `apikey.json`. Produces `IBMQquantum/output/ibm_quantum_validation.png` and `table_ibm_quantum_validation.csv`.
- Hardware used: IBM `ibm_torino` (133 superconducting transmon qubits), accessed via Qiskit Runtime (qiskit 2.3.0, qiskit-ibm-runtime 0.45.0).

The complete simulation code (Python/QuTiP), robustness test scripts, and IBM Quantum validation code, including the scripts that generate all figures and tables reported in this work, are publicly available at: <https://github.com/gabgiani/paw-toymodel>